Supporting Information

Single-Atom Cocatalysts Engineer Proton Microenvironments for Efficient Alkaline Hydrogen Evolution

Guang Yang[a, b, 1], Minghao Yang[a, b, 1], Zeshuo Meng [a, b], Yi Cui[a, b, *]

[a] School of Nano Technology and Nano Bionics, University of Science and Technology of China, Hefei 230026, China

[b] i-lab, Nano-X Vacuum Interconnected Workstation, Suzhou Institute of Nano-Tech and Nano-Bionics, Chinese Academy of Sciences, Suzhou 215123, China

[1] These authors contributed equally: Guang Yang, Minghao Yang.

E-mail: ycui2015@sinano.ac.cn (Yi. Cui)

1. Experimental

1.1 Materials

Molybdenum chloride ($MoCl_5$ 99.6%, Aladdin), Tungsten chloride (WCl_6 99%, Aladdin), Chromium chloride hexahydrate ($CrCl_3 \cdot 6H_2O$, Sinopharm Chemical Reagent), Ruthenium chloride anhydrous ($RuCl_3 \cdot xH_2O$ 99.9%, TCL), Ammonium hydroxide (29%，Adamas), Hydrochloric acid (37%，Adamas), Ethanol (≥99.5%, Sigma-Aldrich), Carbon nanotubes (CNT, Suzhou Tanfeng Graphene Technology Co., Ltd). All chemicals were used without further purification.

1.2 Synthesis of Ru–Mo@CNT, W-Ru@CNT, Cr-Ru@CNT and Ru@CNT

Typically, 0.2 mmol of the respective metal chloride (molybdenum chloride, tungsten chloride, or chromium(III) chloride hexahydrate) and 15 mg of $RuCl_3 \cdot xH_2O$ were dispersed in 10 mL of ethanol and stirred at 40 °C for 10 min. Subsequently, 150 mg of carbon nanotube powder was added, and the mixture was stirred at 40 °C for 4 h, followed by further stirring at 80 °C for another 4 h. The resulting mixture was then dried and subjected to thermal treatment in a tube furnace at 650 °C under an Ar atmosphere for 4 h. To remove unstable components, the obtained sample was sequentially etched by stirring in 1 M HCl and then in 1 M ammonia solution, each for 12 h. The final product was collected by centrifugation and dried, yielding Ru–Mo@CNT, W-Ru@CNT, and Cr-Ru@CNT. For comparison, Ru@CNT was prepared following the same procedure without the addition of any molybdenum, tungsten, or chromium salts.

1.3 Characterization

XRD pattern was recorded on a Bruker AXS D8 Advance X-ray diffractometer with a Cu Ka radiation target (40 V, 40 A). TEM characterization was performed using an FEI Tecnai G2F20 microscope. Atomic-level HAADF-STEM images and the corresponding STEM-EDS elemental maps were measured on an FEI Titan Themis Z 3.1 equipped with a SCOR spherical aberration corrector and a monochromator. The probe convergence angle was 80 mrad, and camera length was 115 mm in the STEM

mode. The morphologies were observed by scanning electron microscopy (SEM, Hitachi model (SU8010). The surface elements were identified by X-ray photoelectron spectroscopy (XPS, Thermo Fisher ESCALAB-250Xi) with monochromatic Al Kα radiation. The chemical bonds were investigated by Raman spectroscopy (Renishaw) equipped with an excitation light source of 532 nm. Py-IR was conducted using a Nicolet 380 FT-IR (Thermo Co., USA) instrument equipped with a custom-made IR cell connected to a vacuum adsorption apparatus. The sample was directly pressed to form a thin wafer and mounted in the transmission vacuum chamber. The sample was evacuated to 10-2 Pa at 323 K for 2 h and cooled to room temperature. Pyridine vapor was injected into the vacuum chamber at room temperature. After reaching adsorption equilibrium, the sample was heated to 323 K and maintained for 1 h to desorb pyridine, and then cooled to room temperature. TOF-SIMS measurement was performed on a TOF-SIMS 5-100 instrument (ION-TOF GmbH) using a 30-keV Bi^{3+} as analysis beam for negative and positive polarity measurements. The weight ratios of Mo, W, Cr and Ru elements in Ru–Mo@CNT, W-Ru@CNT, and Cr-Ru@CNT were measured by the ICP-OES measurements (Thermofisher Avio 200).Ru K-edge and Mo K-edge X-ray adsorption spectra including XANES and EXAFS profiles were collected at BL11B station at the Shanghai Synchrotron Radiation Facility (SSRF).

1.4 Electrochemical measurements

HER electrocatalysis under open conditions.The HER performance was performed on a CHI760E electrochemical station (Shanghai Chenhua Co., China) using a standard three-electrode system in 1 M KOH electrolyte, in which a glassy carbon (GC) electrode (diameter: 3 mm), Hg/HgO electrode, and a carbon rod were used as working, reference, and counter electrodes, respectively. All potentials were recorded against the Hg/HgO electrode and calibrated with respect to a reversible hydrogen electrode (RHE) in accordance with the equation ($E_{RHE} = E_{Hg/HgO}$+0.924 V). In a typical synthesis of the catalyst ink, 3 mg of M-Ru@CNT (M = Mo/W/Cr) was dispersed in a mixture of of 400μL ethanol, 60 μL water, and 40 μL Nafion, followed by sonication for at least 30 min to form a homogeneous ink. Then, 20 μL of the catalyst ink was dropped onto the

polished working electrode and dried naturally for further measurements. LSV curves were collected in 1.0 M KOH at a scan rate of 5 mV s-1 to evaluate the catalytic activity. To ensure accurate iR correction, the solution resistance (R_S) for each sample was first determined via electrochemical impedance spectroscopy (EIS) by fitting the high-frequency intercept of the Nyquist plot using an equivalent circuit (typically a modified Randles circuit). Subsequently, all LSV measurements were subjected to 95% iR compensation, and the compensation level was validated for each individual LSV scan to confirm its appropriateness under the given experimental conditions. The EIS measurement was carried out at frequency ranging from 0.01 Hz to 100 kHz at different potential with a scan rate of 5 mV/s. The electrochemical surface areas (ECSAs) were evaluated from the electrochemical double layer capacitance (C_{dl}) with a potential range from -0.7 ~ -0.8 V versus Hg/HgO at different scan rates. The electrochemical durability was evaluated from chronoamperometry measurements and CV cycling.

TOF calculations. The H_2 conversion efficiencies of samples can be evaluated from the TOF values, which were obtained according to the following equation:

$$TOF\ (s^{-1}) = \frac{j}{2Fn}$$

where j (A) is the current at a given overpotential, 2 is the number of electrons consumed to form 1 mol H_2, F represents the Faraday constant (96500 C/mol), n (mol) is the number of moles of loaded metals, which can be evaluated based on the analysis of ICP-OES measurements.

Definition of degradation rate of voltage (D_V):

$$D_v = \frac{V_2 - V_1}{t}$$

Where V_1 and V_2 are the average potentials during the initial 10% and final 10% of the chronopotentiometry test time, respectively, and t is the total test duration. D_V indicates the increased rate of potential and stands for the total energy consumption during long-term electrolysis.

1.5 DFT Computational

Our simulations were performed within the framework of density functional theory (DFT) implemented in the Quantum Espresso package (QE). The exchange-correlation energies were described using the generalized gradient approximation (GGA) with the Perdew-Burke-Ernzerhof (PBE) functional. To achieve a balance between computational effort and accuracy, energy cutoff is set to 60 Ry for the wave function and 180 Ry for the charge density to generate ground-state eigenvalues, and 160 Ry for the charge density. The geometry relaxation was performed using BFGS quasi-Newton algorithm until the forces on each atom were less than 0.01 eV/Å and the energy difference of consecutive steps was less than 10^{-5} eV. The 10 × 10 graphene supercell was adopted to construct the structures of Mo-Ru@CNT, W-Ru@CNT, Cr-Ru@CNT and Ru@CNT models. The Brillouin-zone sampling were conducted using Monkhorst-Pack (MP) grids of special points with the separation of 0.03 $Å^{-1}$. For the structural optimization and the electronic structure calculations, respectively. A vacuum height of 20 Å along the vertical direction was selected to avoid the unwanted interaction between the slab and its period images. The van der Waals interactions were taken into account using the DFT-D3 approach. The free energy for H* adsorption on a catalyst surface has been widely used to evaluate both H* adsorption and H_2 desorption. The Gibbs free energy of H adsorption was calculated as $\Delta G_{H^*} = \Delta E_{H^*} + \Delta E_{ZPE} - T\Delta S$, where ΔE_{H^*}, ΔE_{ZPE}, and ΔS represent the hydrogen adsorption energy, zero-point energy, and entropy difference defined by a formula $\Delta S = S(H^*) - 1/2 \cdot S(H_2)$, respectively. Here, $S(H^*)$ and $S(H_2)$ represent the entropies of the adsorbed H atom and H_2 in the gas phase at standard conditions, respectively, and the former is approximately zero.

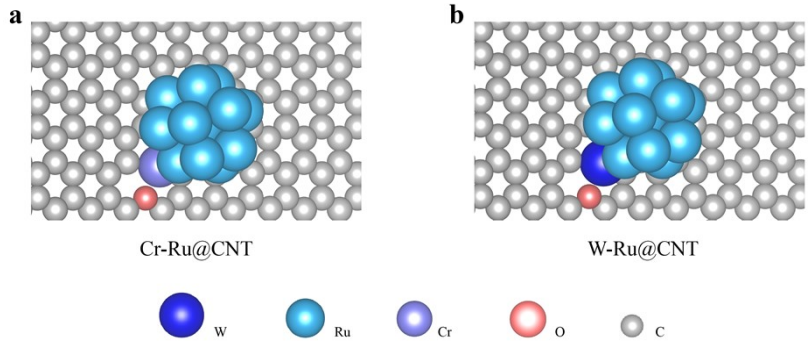

Figure S1. Structural model of Cr-Ru@CNT. (b) Structural model of W-Ru@CNT.

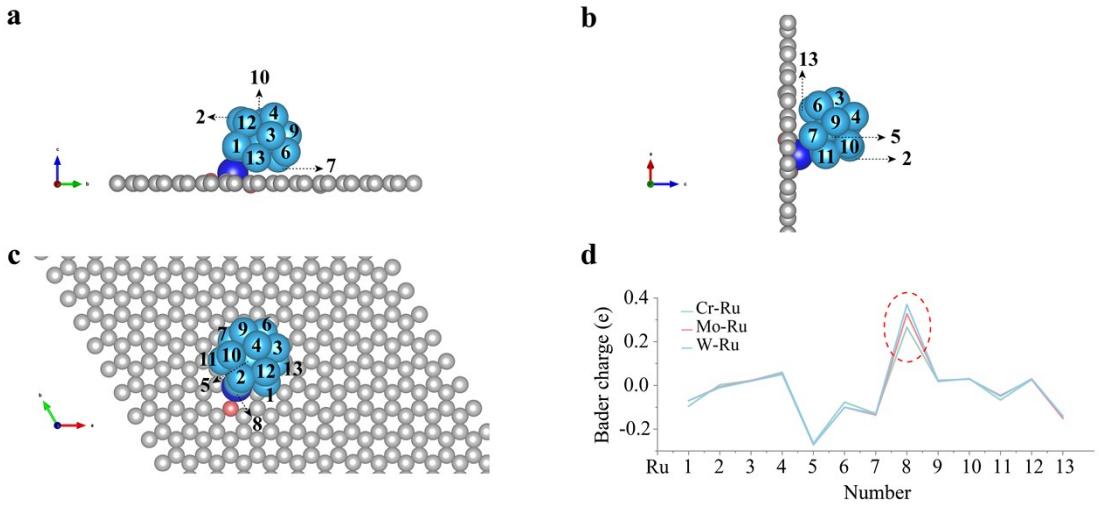

Figure S2. (a) Side view and (b) front view of the Ru_{13} cluster anchored on carbon substrate. (c) Top view of the Ru_{13} cluster on CNT surface with atom numbering. (d) Bader charge distribution of Ru atoms in Cr–Ru, Mo–Ru, and W–Ru models, highlighting charge modulation at the Ru(8) site.

Table S1. ICP-OES measurements for Ru, Mo, Cr and W in Ru–Mo@CNT, Cr-Ru@CNT, and W-Ru@CNT catalysts.

Elements (wt%) / Sample	Ru	Mo	Cr	W
Ru–Mo@CNT	0.4904%	0.0601%		
Cr-Ru@CNT	0.7922%		0.9024%	
W-Ru@CNT	0.6010%			0.1785%

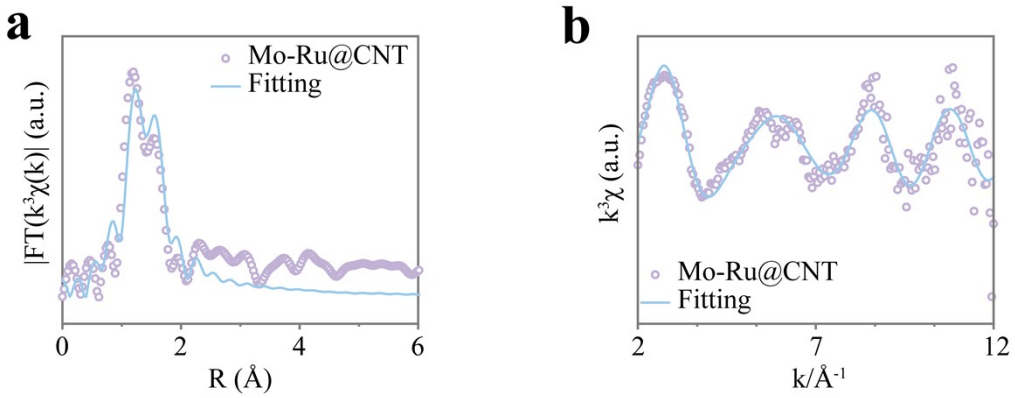

Figure S3. (a) EXAFS R-space fitting curves of Mo-Ru@CNT. (b) EXAFS k-space fitting curves of Mo-Ru@CNT.

Table S2. Structural parameters for Mo-Ru@CNT samples extracted from the Mo K-edge EXAFS fitting. Here, 'Shell' is the bonding type, 'CN' is the coordination number of the Mo atom, 'R'(Å) is the fitting bonding length, 'σ^2' represents the Debye-Waller factor, and the R-factor is used to evaluate the quality of the fitting results.

Sample	Shell	CN	R	σ^2	R-factor
Mo-Ru@CNT	Mo-C	2.177	1.92349	0.00806	0.0048328
	Mo-O	2.120	1.75146	0.00001	

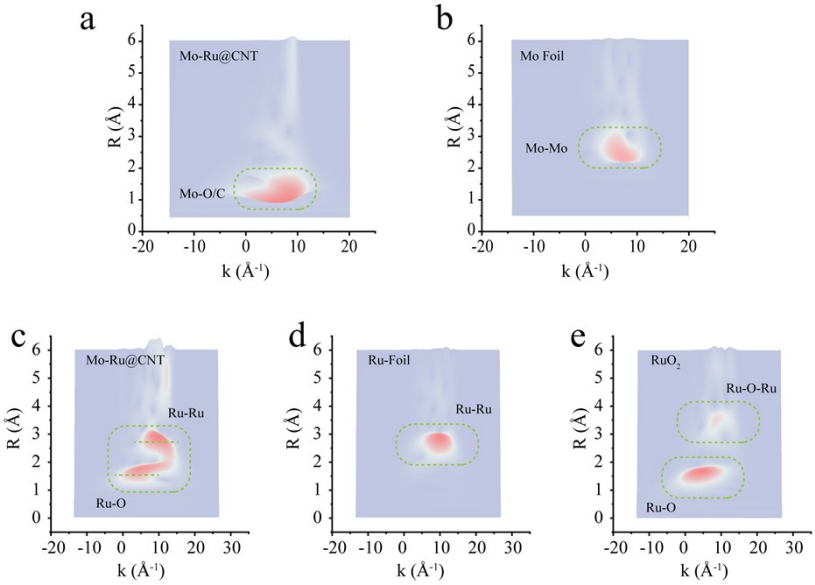

Figure S4. WT-EXAFS spectra of (a) Mo-Ru@CNT (Mo K-edge), (b) Mo foil, (c) Mo-Ru@CNT (Ru K-edge), (d) Ru foil, and (e) RuO_2 reference.

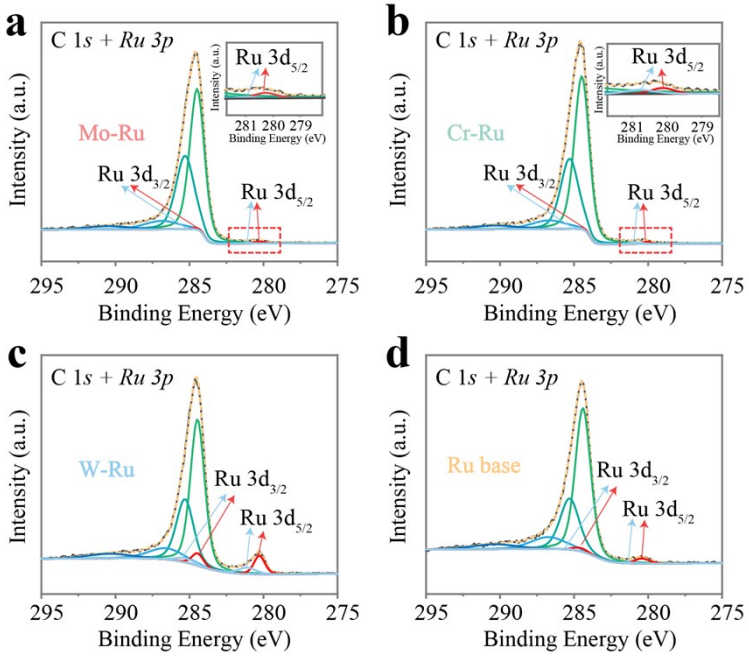

Figure S5. XPS spectra of the C 1*s* + Ru 3*d* region and the fitted Ru 3d peaks for (a) Mo–Ru, (b) Cr–Ru, (c) W–Ru, and (d) Ru-based samples. The Ru $3d_{3/2}$ and Ru $3d_{5/2}$ peaks are labeled in each panel.

Table S3. Binding energies of metallic Ru and oxidized Ru species derived from the Ru $3d_{5/2}$ XPS spectra of different samples.

Sample	Metallic Ru (eV)	Oxidized Ru (eV)
Mo-Ru@CNT	280.595	281.275
Cr-Ru@CNT	280.445	281.105
W-Ru@CNT	280.622	281.462
Ru@CNT	280.822	281.725

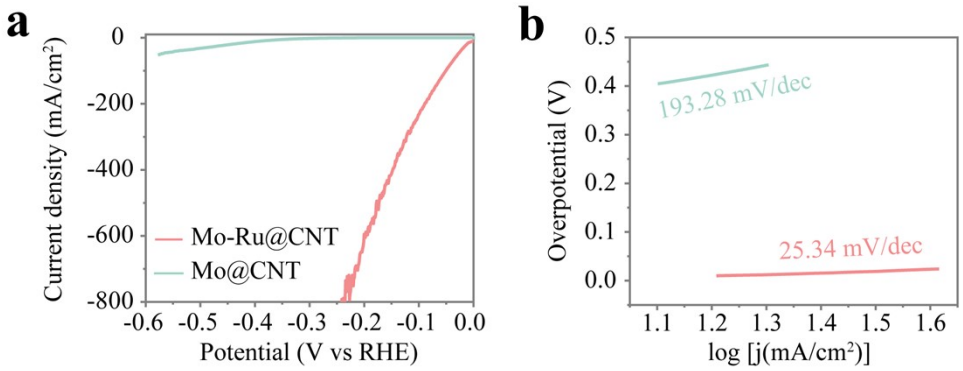

Figure S6. (a) LSV polarization curves and (b) Tafel plots of Mo-Ru@CNT and Mo@CNT.

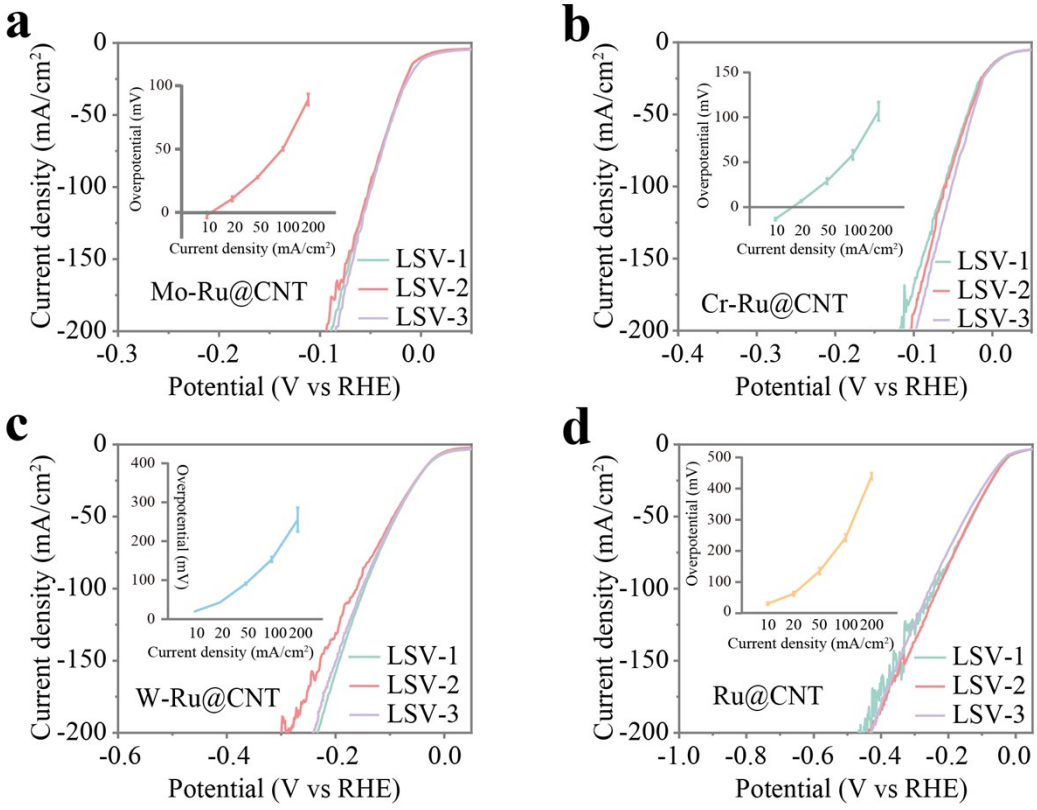

Figure S7. LSV curves of different catalysts: (a) Mo–Ru@CNT, (b) Cr–Ru@CNT, (c) W–Ru@CNT, and (d) Ru@CNT, each measured three times for reproducibility. Insets show the corresponding overpotentials at different current densities with error bars.

Table S4: Average Overpotentials and Error Values of Different Samples at Various Current Densities

Sample / Overpotential	Mo-Ru@CNT	Cr-Ru@CNT	W-Ru@CNT	Ru@CNT
η_{10}	-2.08±2.07	-13.21±1.16	19.29±1.11	30.42±3.64
η_{20}	10.90±1.57	6.68±0.96	42.67±0.36	62.70±5.18
η_{50}	27.86±0.59	28.98±2.65	91.10±1.88	135.62±8.43
η_{100}	50.24±1.12	58.24±4.47	153.43±5.61	242.55±9.48
η_{200}	89.13±3.67	106.93±8.59	255.52±25.30	439.83±8.46

Table S5. Summary of the impedance fitting datas for M-Ru@CNT and Ru@CNT electrodes in 1 M KOH. Here, R_1 is related to the overall electron transfer, R_2 is related to the charge transfer in the interface reaction, R_3 is related to the process of promoting the accumulation of surface hydrogen species.

Catalyst	Rs	R_1	R_2	R_3
Ru-Mo@CNT	9.044	18.409	0.318	2.793
Cr-Ru@CNT	8.914	2.518	1.882	4.565
W-Ru@CNT	7.143	19.957	15.817	17.575
Ru@CNT	13.462	115.129	3.443	28.327

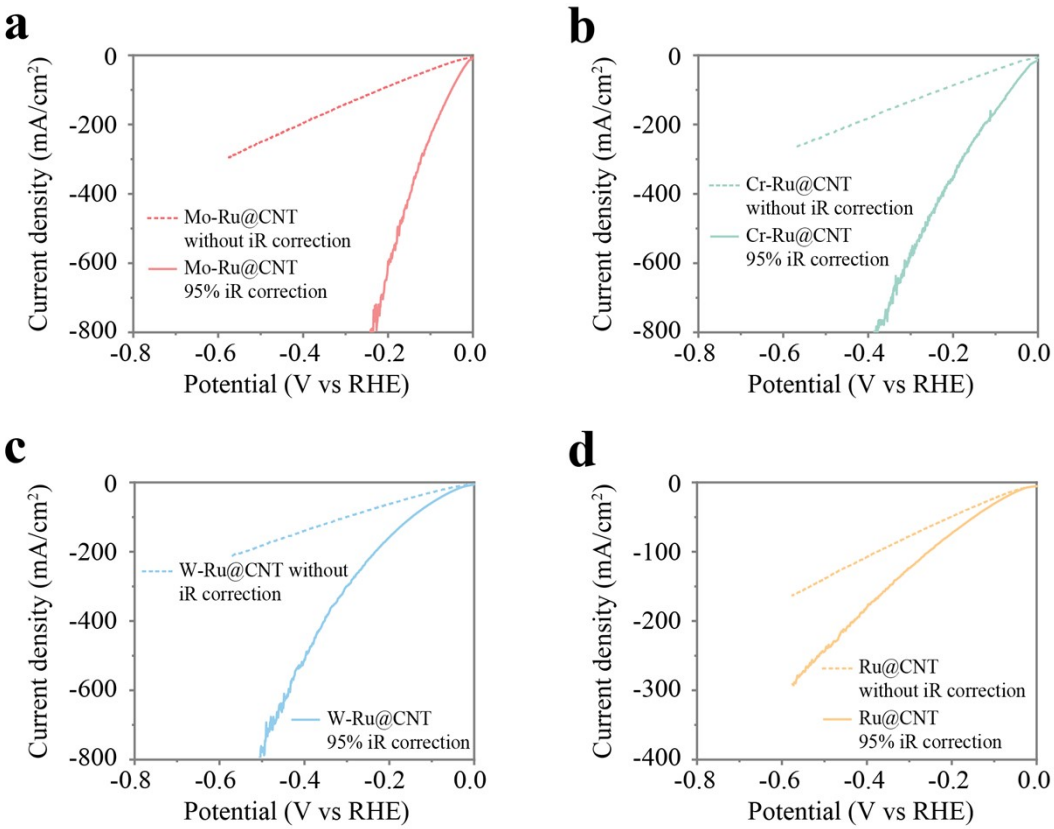

Figure S8. LSV Polarization curves of (a) Mo-Ru@CNT, (b) Cr-Ru@CNT, (c) W-Ru@CNT, and (d) Ru@CNT with and without 95% iR correction. Solid and dashed lines represent corrected and uncorrected data, respectively.

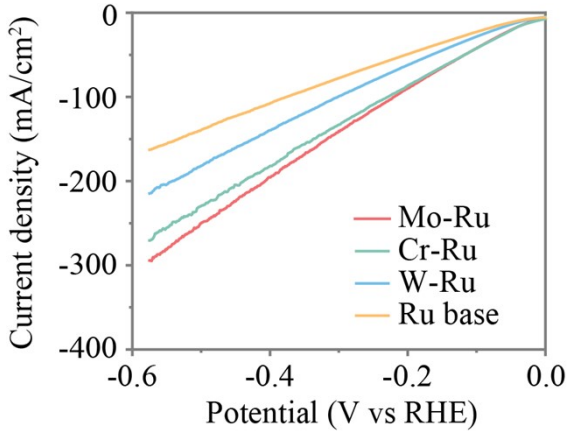

Figure S9 LSV polarization curves without iR correction.

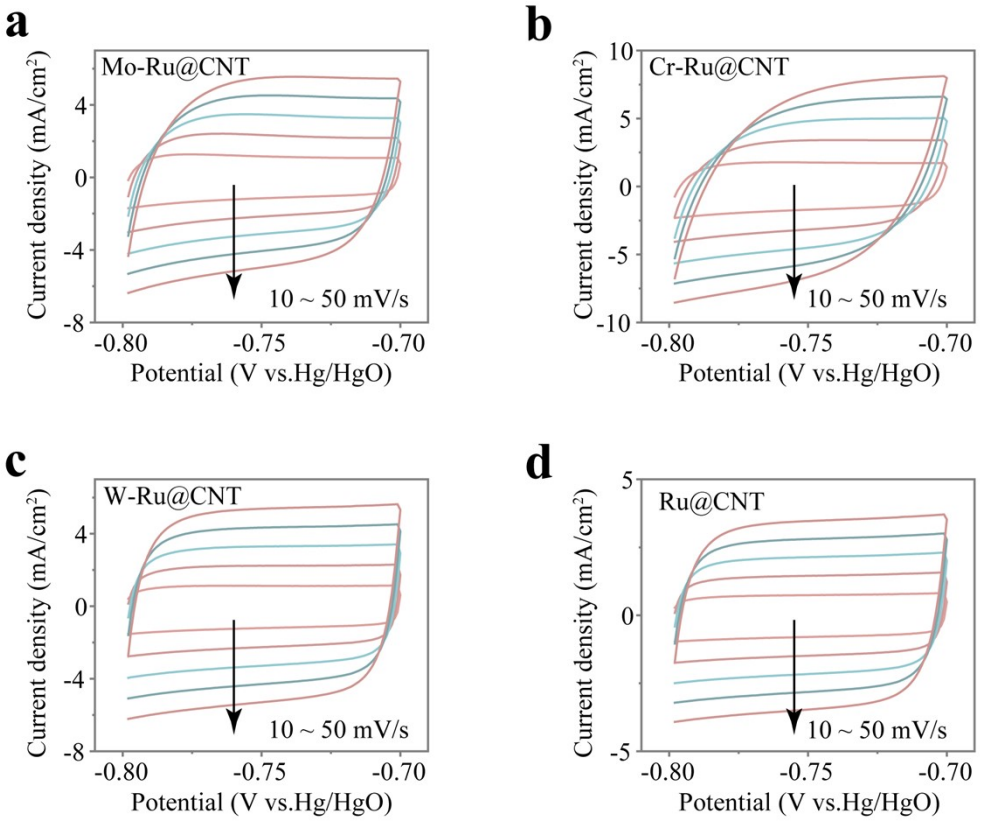

Figure S10. Cyclic voltammetry (CV) measurements of the different catalysts in 1.0 M KOH alkaline electrolyte of (a) Mo-Ru@CNT, (b) Cr-Mo@CNT (c) W-Mo@CNT, (d) Ru@CNT in the voltage window from -0.8 to -0.7 V vs. Hg/HgO at the scan rates of 10-50 mV/s.

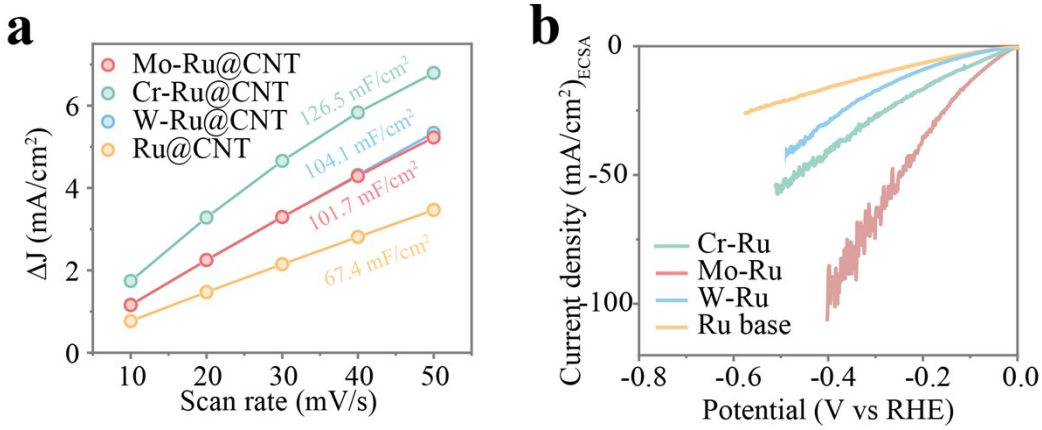

Figure S11. (a) Double layer capacitance comparisons of Mo-Ru@CNT and reference catalysts，(b) ECSA-normalized LSV polarization curves.

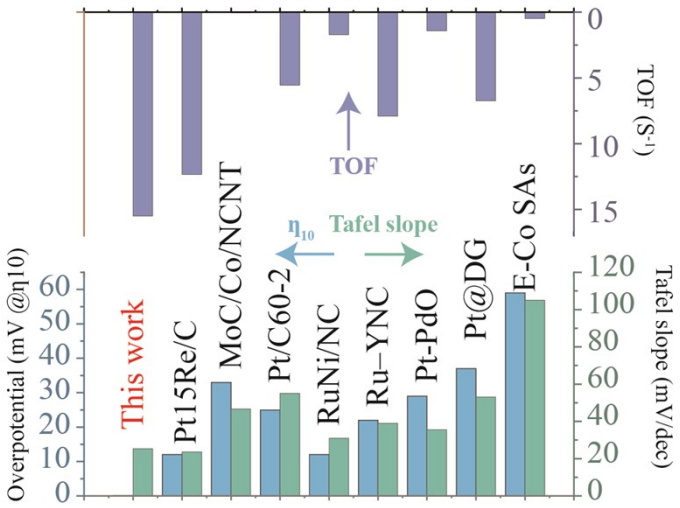

Figure S12. Benchmark comparison of overpotential at 10 mA cm^{-2}, Tafel slope, and turnover frequency (TOF at 100 mV) for the Mo–Ru@CNT catalyst and previously reported state-of-the-art HER catalysts in 1 M KOH.

Table S6. Comparison of overpotentials (10 mA/cm^2 and 100 mA/cm^2), Tafel slopes, TOF (@100 mV) and stability of Mo-Ru@CNT catalyst and previously reported excellent HER catalysts in 1 M KOH alkaline electrolyte solutions.

Catalysts	**η_{10} (mV)**	**η_{100} (mV)**	**Tafel slope (mV/dec)**	**TOF (s^{-1})**	**Stability (h)**	**Reference**
This Work	0	50.24	25.34	15.49	200 (η_{500})	**This work**
$Pt_{15}Re/C$	12		23.6	12.34	183 (η_{10})	Chem. Eng. J., 2026, 532: 174149.
Co-$P_{0.43}$@NF		141	85	5.64	150 (η_{500})	Adv.Funct.Mater. 2024, 34, 2410825
FeOOH/Mo-NiS_x,		162	92	＜5	200 (η_{100})	ACS Catal. 2026, 16, 4631−4645
MoC/Co/NC NT	33		46.7	0.05	16.7 (η_{10})	ACS Catal. 2025, 15, 14983−14995
Pt/C_{60}-2	25		55	5.55	100 (η_{10})	Nat. Commun., 2023, 14: 2464.
RuNi/NC	12	66	30.9	1.70	1600 (η_{10})	Nat. Commun., 2024, 15: 7179
Ru–YNC	22	109	39	7.9	200 (η_{10})	Energy Environ. Sci., 2025, 18, 6141–6153
Pt-PdO	29		35.6	1.42	36 (η_{10})	ACS Sustainable Chem. Eng. 2022, 10, 3704−3715
Pt@DG	37		53	6.74	8.3 (η_{10})	J. Am. Chem. Soc. 2022, 144, 2171−2178
E-Co SAs	59		105	0.48	500 (η_{10})	Adv. Funct. Mater. 2021, 31, 2100547

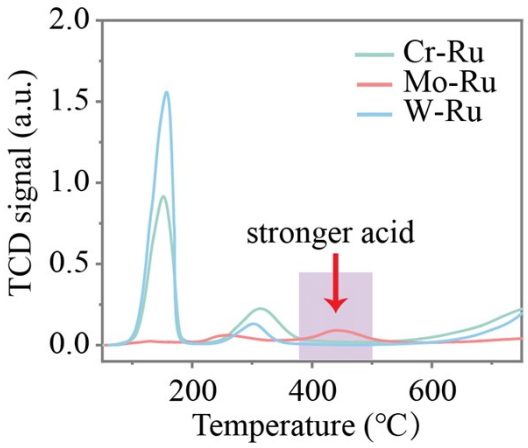

Figure S13. NH_3-TPD profiles of different catalysts showing that Mo-Ru@CNT exhibits a stronger high-temperature desorption peak, indicating stronger acid-site strength compared to Cr-Ru@CNT and W-Ru@CNT.

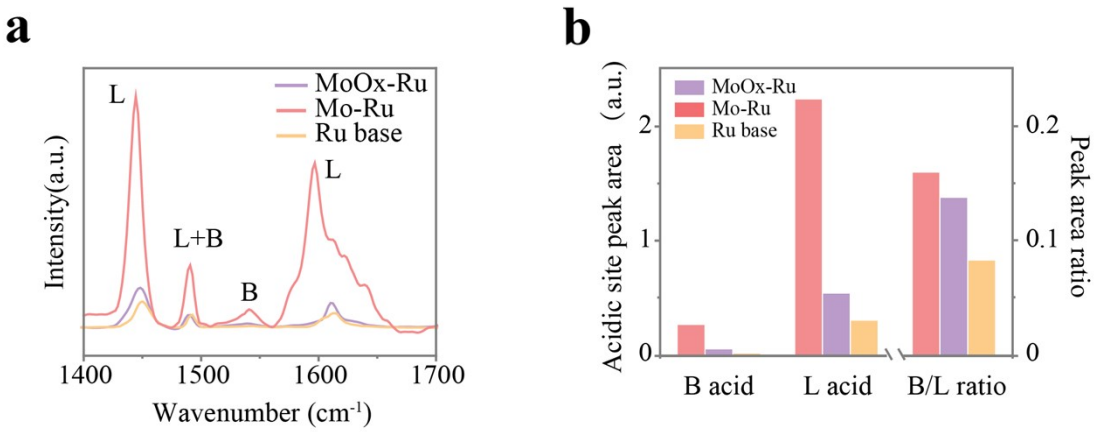

Figure S14. (a) Pyridine-IR spectra of Mo-Ru@CNT, MoOx-Ru@CNT, and Ru@CNT after electrochemical treatment. (b) Quantitative analysis of Brønsted and Lewis acid sites.

Table S7. The peak areas of Lewis (L) and Brønsted (B) acid sites and their peak area ratios (B/L) for M-Ru@CNT, MoOx-Ru@CNT and Ru@CNT catalysts.

Sample	L acid area	B acid area	Peak area ratio (B/L)
Mo-Ru@CNT	2.226	0.267	0.158802
Cr-Ru@CNT	1.888	0.124	0.086954
W-Ru@CNT	1.524	0.112	0.097298
MoOx-Ru@CNT	0.54	0.056	0.137298
Ru@CNT	0.305	0.019	0.082475

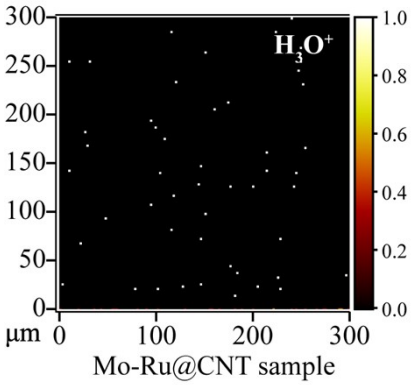

Figure S15. 2D TOF-SIMs mapping of hydronium ion (H_3O^+) distribution on Mo-Ru@CNT surface.

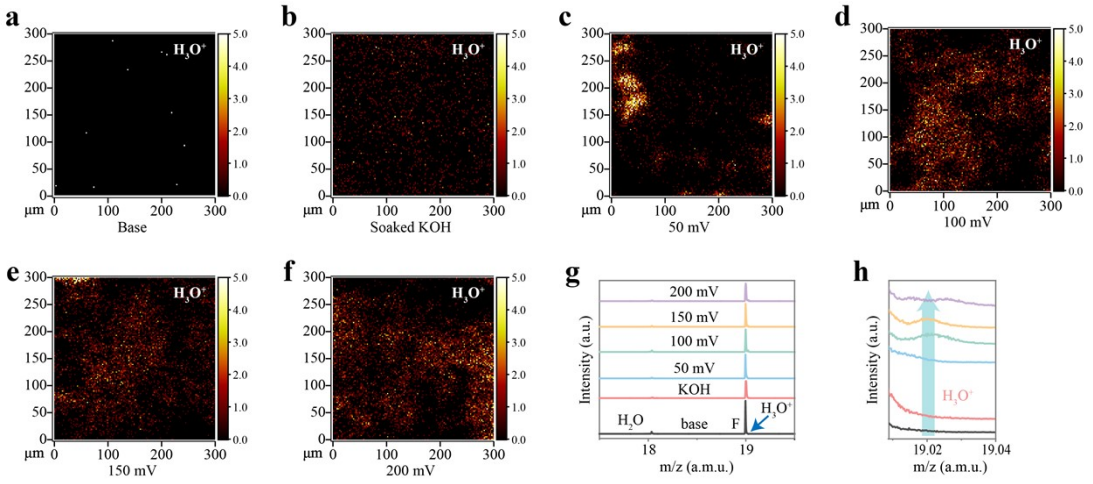

Figure S16. Quasi-in-situ TOF-SIMS analysis: (a-f) 2D TOF-SIMS images (H_3O^+) of the Mo-Ru@CNT single-atom catalyst at different overpotentials, (g-h) TOF-SIMS spectra.

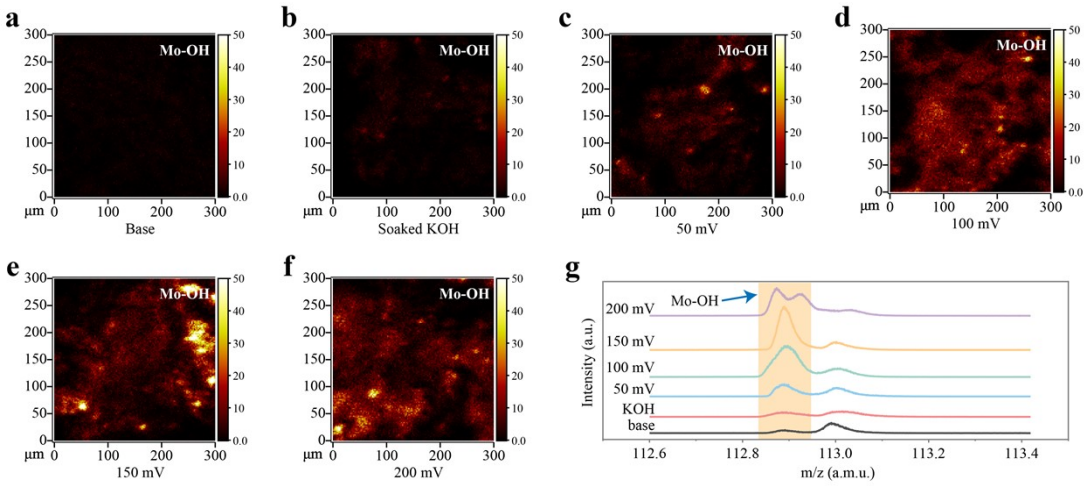

Figure S17. Quasi-in-situ TOF-SIMS analysis: (a–f) 2D TOF-SIMS images (Mo-OH) of the Mo-Ru@CNT single-atom catalyst at different overpotentials, (g) TOF-SIMS spectra.

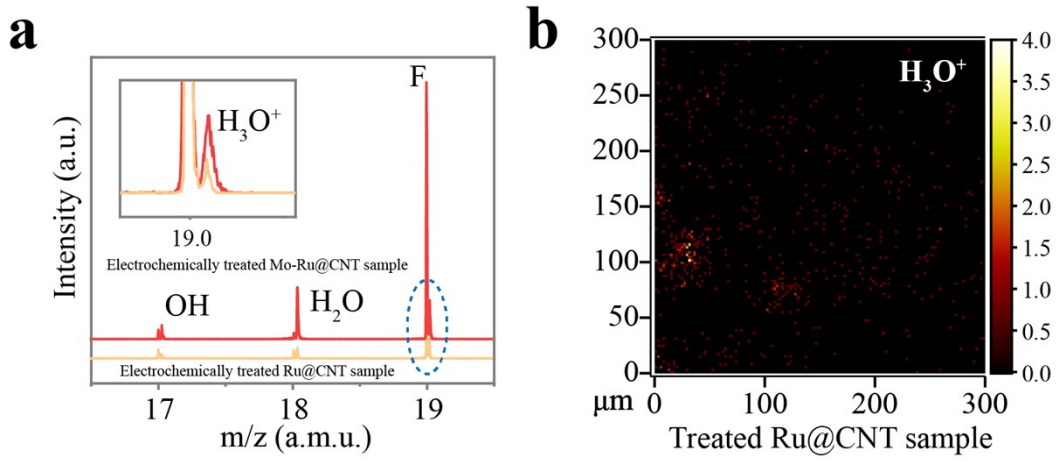

Figure S18. (a) TOF-SIMs plots of Electrochemically treated Ru@CNT and Mo-Ru@CNT samples, (b) TOF-SIMs mapping of hydronium ion (H_3O^+) distribution on the treated Ru@CNT surface.